PHYSICAL REVIEW B **78**, 180410(R) (2008)

Chiral spin states in the pyrochlore Heisenberg magnet: Fermionic mean-field theory and variational Monte Carlo calculations

Jung Hoon Kim and Jung Hoon Han*

Department of Physics, BK21 Physics Research Division, Sungkyunkwan University, Suwon 440-746, Republic of Korea

(Received 16 July 2008; revised manuscript received 28 September 2008; published 14 November 2008)

Fermionic mean-field theory and variational Monte Carlo calculations are employed to shed light on the possible uniform ground states of the Heisenberg model on the pyrochlore lattice. Among the various flux configurations, we find the chiral spin states carrying $\pm\pi/2$ flux through each triangular face to be the most stable both within the mean-field theory and the projected wave-function studies. Properties of the spin-spin correlation function and the chirality order parameter are calculated for the projected wave functions. Mean-field band structures are examined.

DOI: 10.1103/PhysRevB.78.180410 PACS number(s): 75.10.Jm, 75.50.Ee

I. INTRODUCTION

The question of the quantum ground state of spin-1/2 Heisenberg Hamiltonian

$$H = \sum_{\langle ij \rangle} \mathbf{S}_i \cdot \mathbf{S}_j \tag{1}$$

on the pyrochlore lattice has prompted active research for nearly two decades.[1–6] A popular scheme, employed in Refs. 1–4, was to solve the isolated tetrahedron problem exactly and to couple the nearby disjoint tetrahedra in the weak exchange energy J'. A nonmagnetic state with exponentially short correlation length was identified in Ref. 1 in this way, and Refs. 2–4 noted the dimer instability in the ground state. A similar dimer instability was discovered in the large-N approach in Ref. 5. While Refs. 2–4 begin with the dimer basis of a single-tetrahedron solution to carry out perturbation in J', Ref. 5 starts with a translationally invariant solution and finds that dimerization occurs as a spontaneous symmetry breaking.

In this Rapid Communication, we adopt the fermionic mean field followed by variational Monte Carlo (VMC) treatment to address this issue. Prior work in the same spirit for the Kagome lattice can be found in Ref. 7. We find chiral spin states[8] with nonzero averages of the three-spin operator $\langle \mathbf{S}_i \cdot \mathbf{S}_j \times \mathbf{S}_k \rangle$ for the elementary triangular unit formed by $\langle ijk \rangle$ sites to be the likely nonmagnetic ground state of the Heisenberg model realized on pyrochlore lattice under the assumption of uniform nearest-neighbor bond amplitudes $|\langle \mathbf{S}_i \cdot \mathbf{S}_j \rangle|$. The flux through the triangles are found to be $\pm\pi/2$ at the mean-field level but reached a smaller value after the Gutzwiller projection was carried out.

II. MEAN-FIELD THEORY

In rewriting the spin operator as a fermion bilinear and introducing the mean-field variable $\chi_{ij} = \langle f_i^+ f_j \rangle$, one arrives at the mean-field Hamiltonian

$$H_{\mathrm{MF}} = -\sum_i \sum_{j \in i} \chi_{ij}^* f_i^+ f_j + \sum_i \lambda_i (f_i^+ f_i - 1/2), \tag{2}$$

with the Lagrange multiplier λ_i enforcing the occupation constraint at each site. In doing the mean-field calculation we drop the spin index and work with the half-filled case $\langle f_i^+ f_i \rangle = 1/2$. The summation over all nearest-neighbor sites j with respect to i is indicated by $\Sigma_{j \in i}$. To set up the coordinates, we place the four corners of a single "up" tetrahedron (uT) at (0,0,0), (1,0,0), $(1/2, \sqrt{3}/2, 0)$, and $(1/2, 1/2\sqrt{3}, \sqrt{2/3})$ then displace it by integer combinations of $\hat{e}_1 = (2,0,0)$, $\hat{e}_2 = (1, \sqrt{3}, 0)$, and $\hat{e}_3 = (1, 1/\sqrt{3}, \sqrt{8/3})$ to generate the pyrochlore lattice: $n_1 \hat{e}_1 + n_2 \hat{e}_2 + n_3 \hat{e}_3$, n_i = integers. Each uT is met at four corners by down tetrahedra (dT) and vice versa as shown in Fig. 1. The self-consistent mean-field calculations were run for $L \times L \times L \equiv L^3$ lattice with $4L^3$ lattice sites. L refers to the number of uT's along each $\hat{e}_\alpha$ direction. The lattice contains an equal number of uT and dT blocks.

A completely unrestricted minimization of $\langle H_{\mathrm{MF}} \rangle$ resulted in the ground state with each site paired into a dimer while all dimers are disconnected from one another, in accordance with Rokhsar's[9] general observation. The extensive degeneracy of the dimer ground state will be lifted at higher orders in $1/N$ in a large-N expansion to give rise to a ground state with (possibly) restored translational symmetry. Furthermore, the fully dimerized state carries an energy of -0.375 per site, which is much higher than some of the uniform states we consider in this Rapid Communication. Therefore, we move with the idea that the true ground state of Eq. (1) is better captured by the uniform amplitude ansatz $|\chi_{ij}| = \chi$ but with arbitrary phases: $\chi_{ij} = \chi e^{i\phi_{ij}}$. For a single tetrahedron, such a search yielded solutions where the flux through the four triangular faces are all equal to $\Phi = +\pi/2$ or $-\pi/2$. The flux is defined from the directed product $e^{i\Phi} = e^{i[\phi_{ij} + \phi_{jk} + \phi_{ki}]}$ as the three sites of a triangle $\langle ijk \rangle$ are traversed in a counterclockwise (CCW) manner when viewed from outside the tetrahedron. For the lattice problem with uniform $|\chi_{ij}|$, the mean-field ground state is found to be the one with staggered chirality: $\Phi = \pi/2$ for all the uT's and $\Phi = -\pi/2$ for all the dT's or vice versa. No solutions were found where different faces of a given tetrahedron, either up or down, carried different amounts of flux or flux other than $\pm\pi/2$. The fluxes through the hexagons of the pyrochlore lattice were all zero. The mean-field ground-state solution is in complete conformity with the "Rokhsar rule"[10] of the flux for different types of polygons.

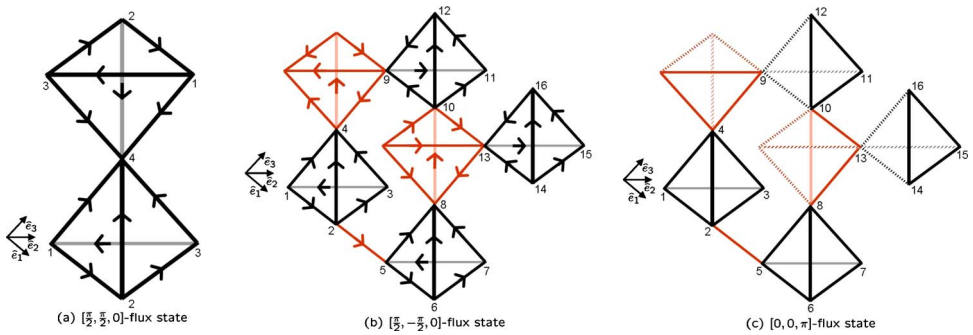

FIG. 1. (Color online) χ_{ij} bond configurations producing (a) $[\frac{\pi}{2},\frac{\pi}{2},0]$, (b) $[\frac{\pi}{2},-\frac{\pi}{2},0]$, and (c) $[0,0,\pi]$ flux states. Setting $|\chi_{ij}|=1$, the direction of the arrows indicates $\chi_{ij}=+i$ going from i to j. The shaded bonds are lying on the back sides. Independent sites are labeled from 1 through 4 (one up tetrahedron in a unit cell) in (a) and from 1 through 16 (four up tetrahedra in a unit cell) in (b) and (c). In (c), the thick (dotted) lines represent bonds with $\chi_{ij}=1(-1)$.

III. VARIATIONAL MONTE CARLO CALCULATION

VMC calculations of the energies of several mean-field ansatz states were carried out including the one found in the mean-field calculation. The states are labeled by [uT, dT, H], where the three numbers uT, dT, and H refer to the flux through the triangles of the up tetrahedra, down tetrahedra, and the hexagons, respectively. We examine four such states: (i) [0,0,0], (ii) $[\frac{\pi}{2},\frac{\pi}{2},0]$, (iii) $[\frac{\pi}{2},-\frac{\pi}{2},0]$, and (iv) $[0,0,\pi]$. The mean-field result corresponds to case (iii). For future reference, we denote (ii) and (iii) as uniform and staggered flux states. The other two states, (i) and (iv), do not break time-reversal symmetry. The choices of the trial states are motivated by and parallel those in Ref. 7 for the Kagome lattice. The χ_{ij} bond patterns that generate each state at the mean-field level are shown in Fig. 1. With χ_{ij}'s given in Fig. 1 as input to Eq. (2) one can diagonalize H_{MF} to obtain the mean-field ground state $|\psi_{\mathrm{MF}}\rangle$ as a Slater determinant. The evaluation of the energy and other operators $\hat{X}$ is carried out in the projected space $|s\rangle$ ($|s\rangle$ spans all the states with one spin per site) by

$$\langle\hat{X}\rangle=\frac{\sum_s\langle\psi_{\mathrm{MF}}|s\rangle\langle s|\hat{X}|\psi_{\mathrm{MF}}\rangle}{\sum_s\langle\psi_{\mathrm{MF}}|s\rangle\langle s|\psi_{\mathrm{MF}}\rangle}=\sum_s P(s)\frac{\langle s|\hat{X}|\psi_{\mathrm{MF}}\rangle}{\langle s|\psi_{\mathrm{MF}}\rangle},\qquad(3)$$

where $P(s)=|\langle s|\psi_{\mathrm{MF}}\rangle|^2/\Sigma_s|\langle s|\psi_{\mathrm{MF}}\rangle|^2$ is the probability weight used in the Monte Carlo procedure.[11]

TABLE I. Energy per site of various states obtained from VMC depending on the number of up tetrahedra L in each direction. The two chiral states have much lower energies than the nonchiral states. Statistical uncertainties lie below the digits shown. Boundary conditions, aPBC or PBC, used in the calculation are listed.

L	[0,0,0]	$[\frac{\pi}{2},\frac{\pi}{2},0]$	$[\frac{\pi}{2},-\frac{\pi}{2},0]$	$[0,0,\pi]$
	aPBC	aPBC	PBC	PBC
2	−0.372	−0.478	−0.466	−0.374
4	−0.374	−0.459	−0.456	−0.375

The unit cell includes a single tetrahedron for the [0,0,0] and $[\frac{\pi}{2},\frac{\pi}{2},0]$ states, and $2\times2\times1$ tetrahedra for the $[\frac{\pi}{2},-\frac{\pi}{2},0]$ and $[0,0,\pi]$ states. Periodic boundary conditions (PBCs) generate degenerate states at the Fermi level for the [0,0,0] and $[\frac{\pi}{2},\frac{\pi}{2},0]$ cases, which can be lifted by applying antiperiodic boundary conditions (aPBCs) along one of the directions, e.g., $\hat{e}_1$, for [0,0,0], and along two directions, e.g., $\hat{e}_1$ and $\hat{e}_2$, for $[\frac{\pi}{2},\frac{\pi}{2},0]$. In the case of $[\frac{\pi}{2},-\frac{\pi}{2},0]$ and $[0,0,\pi]$ the unit cell includes four up tetrahedra, two in the $\hat{e}_1$ direction and two in the $\hat{e}_3$ direction, for the χ_{ij} patterns shown in Figs. 1(b) and 1(c). PBC suffices in both these cases since no degeneracy occurs at the Fermi level.

The VMC energies of the trial states we propose are listed in Table I. Several independent Monte Carlo simulations were made with each simulation consisting of over 10^5 steps (each step means one sweep of the whole lattice) for each state to obtain reliable estimates of the energy. Due to the rapid increase in the system size with L, the calculation is currently limited to $L=4$. For L up to 4, the two chiral states turn out to have much lower energies than the two nonchiral states. The energies of the two chiral states are very close.

IV. SPIN-SPIN CORRELATION AND CHIRALITY

The spin-spin correlation function can be computed using the relation $\langle\mathbf{S}_i\cdot\mathbf{S}_j\rangle=(3/4)\langle\sigma_i^z\sigma_j^z\rangle$ due to the spin isotropy of the ground state. Table II displays the spin-spin correlations obtained for all four flux configurations as a function of the distance for $L=4$. We measure the correlation along the six directions, $\hat{e}_1$, $\hat{e}_2$, $\hat{e}_3$, $\hat{e}_1-\hat{e}_2$, $\hat{e}_2-\hat{e}_3$, and $\hat{e}_3-\hat{e}_1$, and take av-

TABLE II. The spin-spin correlation function $\langle\mathbf{S}_i\cdot\mathbf{S}_j\rangle$ with respect to distance for the four flux states. Five independent 10^5 MC steps were used for each data point.

$\lvert i-j\rvert$	[0,0,0]	$[\frac{\pi}{2},\frac{\pi}{2},0]$	$[\frac{\pi}{2},-\frac{\pi}{2},0]$	$[0,0,\pi]$
1	−0.1249(2)	−0.1533(1)	−0.1522(1)	−0.1250(1)
2	+0.0088(3)	+0.0194(2)	+0.0122(1)	−0.0054(3)
3	−0.0027(1)	−0.0129(1)	−0.0024(3)	+0.0012(2)
4	+0.0007(2)	+0.0060(2)	+0.0006(3)	+0.0001(6)

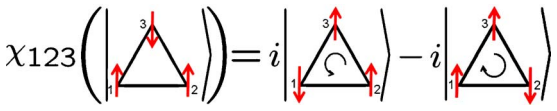

FIG. 2. (Color online) The two states, $|s_+\rangle$ and $|s_-\rangle$, produced by the chirality operation on a state $|s\rangle$.

erages. The results for any one direction are consistent with those taken along any other. It was difficult to reach a large enough size to discriminate an algebraic decay of the correlation against an exponential one. The sign of $\langle \mathbf{S}_i \cdot \mathbf{S}_j \rangle$ alternated with distance as expected in an antiferromagnetically correlated state, except for $[0,0,\pi]$ where the signs of the second- and the third-neighbor correlations are reversed (see Table II). The fast decay of the spin-spin correlation is consistent with an earlier finding of Ref. 1 based on the cluster perturbation method.

Both the mean-field search and the VMC calculation suggest that the chiral states with spontaneously broken time-reversal symmetry ($\mathcal{T}$) are vital in the understanding of the ground-state correlation of the Heisenberg model on the pyrochlore lattice. We develop below an extension of the VMC method which allows the calculation of the chirality and evaluate it for the chiral states.

The scalar chirality $\hat{\chi}_{123}=\langle \mathbf{S}_1 \cdot \mathbf{S}_2 \times \mathbf{S}_3 \rangle$ is equivalent to[8]

$$\frac{1}{2}\mathrm{Im}(\langle \hat{\chi}_{12}\hat{\chi}_{23}\hat{\chi}_{31}\rangle) = \frac{\langle \hat{\chi}_{12}\hat{\chi}_{23}\hat{\chi}_{31} - \hat{\chi}_{13}\hat{\chi}_{32}\hat{\chi}_{21}\rangle}{2i} \tag{4}$$

with $\hat{\chi}_{ij}=\Sigma_\sigma f^+_{i\sigma} f_{j\sigma}$. It is the difference of the cyclic permutation of the spins done in the CCW and clockwise (CW) directions. Unlike in the evaluation of the spin-spin correlation where the action of $\sigma^z_i \sigma^z_j$ on a given basis state $|s\rangle$ is diagonal, the outcome of $\hat{\chi}_{123}|s\rangle$ is not proportional to $|s\rangle$ itself. Instead, we obtain the relation $\hat{\chi}_{123}|s\rangle = i(|s_+\rangle - |s_-\rangle)$, as depicted in Fig. 2. The two states $|s_+\rangle$ and $|s_-\rangle$ are obtained as CCW and CW rotations by one lattice site of the original spin configuration $|s\rangle$ with the rotation axis chosen to point out of the triangular faces of the tetrahedra. When the state $|s\rangle$ contains all three spins up or all down for a given triangle, the chirality operation gives zero. The average $\langle \hat{\chi}_{123} \rangle$ is obtained from

$$\langle \hat{\chi}_{123} \rangle = i \sum_s P(s) \left[\frac{\langle s_- | \psi \rangle - \langle s_+ | \psi \rangle}{\langle s | \psi \rangle} \right]. \tag{5}$$

Here $P(s)$ is the statistical weight $|\langle s|\psi\rangle|^2 / \Sigma_s |\langle s|\psi\rangle|^2$ for a given mean-field state $|\psi\rangle$. Following the usual manner of updating the configuration by Monte Carlo methods, one has to calculate the ratio $(\langle s_-|\psi\rangle - \langle s_+|\psi\rangle)/\langle s|\psi\rangle$ for each state $|s\rangle$.

In the VMC calculation we take averages of $\langle s_-|\psi\rangle/\langle s|\psi\rangle$ and $\langle s_+|\psi\rangle/\langle s|\psi\rangle$ separately. The two quantities turn out to be complex conjugates with extremely high accuracy, so one can denote the averaged $\langle s_+|\psi\rangle/\langle s|\psi\rangle$ and $\langle s_-|\psi\rangle/\langle s|\psi\rangle$ as $\langle \hat{\eta}_{123}\rangle/2 \pm i\langle \hat{\chi}_{123}\rangle/2$, respectively. The flux Φ_{123} is deduced from $\tan(\Phi_{123}) = \langle \hat{\chi}_{123}\rangle / \langle \hat{\eta}_{123}\rangle$. The signs of the flux after the projection turned out to be in perfect accord with the mean-field predictions. On the other hand, the amount of flux is reduced from the mean-field value $\pi/2$ after the projection (see Table III). The chirality was zero within a statistical error for the nonchiral states, $[0,0,0]$ and $[0,0,\pi]$. The increase in the average flux Φ with the system size is consistent with the scenario of a long-range ordering of the chirality in the ground state.

TABLE III. The real and imaginary parts of the averages of $\langle s_+|\psi\rangle/\langle s|\psi\rangle$ and the flux (in units of $\pi/2$) through the triangle for $[\frac{\pi}{2},\frac{\pi}{2},0]$ (left three columns) and $[\frac{\pi}{2},-\frac{\pi}{2},0]$ (right three columns).

L	η_{123}	$\lvert\chi_{123}\rvert$	$\lvert\Phi_{123}\rvert$	η_{123}	$\lvert\chi_{123}\rvert$	$\lvert\Phi_{123}\rvert$
2	0.376	0.356	0.483	0.368	0.325	0.461
4	0.314	0.358	0.542	0.312	0.358	0.544

V. BAND STRUCTURE

The band structures of the four flux configurations in Fig. 1 have been analyzed along the three orthogonal directions k_x, k_y, k_z as well as along k_α that is defined to lie along the three $\hat{e}_\alpha$ directions, $\alpha=1,2,3$. The relations between the two sets of momenta are $k_1=k_x$, $k_2=k_x/2+\sqrt{3}k_y/2$, and $k_3=k_x/2+\sqrt{3}k_y/6+\sqrt{6}k_z/3$. Flat bands lying exactly at E_F were observed in the $[0,0,0]$ and $[\frac{\pi}{2},\frac{\pi}{2},0]$ states, and above E_F for the $[0,0,\pi]$ state. No flat bands exist for $[\frac{\pi}{2},-\frac{\pi}{2},0]$. We describe the respective band structures in more detail. (i) $[0,0,0]$: a twofold-degenerate flat band lies exactly at E_F for each k_α direction. The other two nondegenerate bands lying below E_F are dispersive. (ii) $[\frac{\pi}{2},\frac{\pi}{2},0]$: a twofold-degenerate flat band at $E_F=0$ was observed along the k_z direction, $k_x=k_y=0$. The other two bands are given by $\sim \pm\cos(\sqrt{2/3}k_z)$. Along each of the k_α directions, the uppermost and the lowermost bands (which are related by particle-hole symmetry) are flat, and the other two dispersive bands cross at E_F as k_α equals a multiple of π. There is no gap for this or the $[0,0,0]$ flux configuration. This explains the existence of a Fermi-level degeneracy in the finite-size mean-field energy spectra. (iii) $[\frac{\pi}{2},-\frac{\pi}{2},0]$: four doubly degenerate bands lie below the Fermi level and the others lie above it (separated by an energy gap). Dispersion along the k_α directions is displayed in Fig. 3. (iv) $[0,0,\pi]$: of the 16 bands, the uppermost band lying above E_F is eightfold degenerate and flat along each of

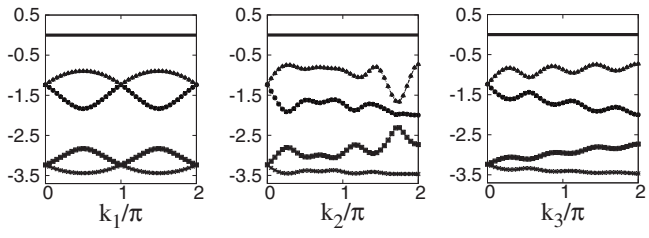

FIG. 3. Mean-field energy bands for the $[\frac{\pi}{2},-\frac{\pi}{2},0]$ state along $k_\alpha=\mathbf{k}\cdot e_\alpha$ directions, $0 \le k_\alpha < 2\pi$. Each band is twofold degenerate. The occupied bands shown here are symmetric with the upper unoccupied bands due to particle-hole symmetry. The horizontal line $E_F=0$ is the Fermi level. Dispersion along other directions (not shown) also shows a full gap.

the k_α directions. The remaining ones are the four twofold-degenerate bands lying below the Fermi level and separated by a gap from the uppermost one. A gap separates the occupied from the empty bands for the $[\frac{\pi}{2},-\frac{\pi}{2},0]$ and $[0,0,\pi]$ flux states, which also explains the absence of a Fermi-level degeneracy in an earlier mean-field calculation.

The presence of flat bands in the [0,0,0] and $[\frac{\pi}{2},\frac{\pi}{2},0]$ flux states over a linear segment of the Brillouin zone suggests that an instability might play a role. In the case of the uniform flux state, the degeneracy-lifting terms are given by the modulation of the bond amplitudes for triangles lying in the plane spanned by $\hat{e}_1$ and $\hat{e}_2$ vectors. Specifically it corresponds to $i\chi \rightarrow i(\chi+\lambda)$ for the (123) triangle of the up tetrahedron, and $i\chi \rightarrow i(\chi-\lambda)$ for the (123) corners of the down tetrahedron shown in Fig. 1(a). The flux through the triangles remains fixed at $\pi/2$. We observed that the introduction of nonzero λ did not decrease the variational energy. Rather there was an increase in the third significant digit of the energy value for λ/χ up to 0.1 and by 2.7% at $\lambda/\chi=0.2$. The slow dependence of the overall energy is partly due to the boundary conditions used, which already opened the gap in the finite-size single-particle spectra. Another reason for the lack of dependence may be the degeneracy is confined to a linear segment of the Brillouin zone, so that not enough states are affected by the degeneracy-lifting mechanism. On the other hand, the gapful nature of the band structures for $[\frac{\pi}{2},-\frac{\pi}{2},0]$ will guarantee stability of the Gutzwiller-projected state against small fluctuations. At the moment we believe both types of flux states have a chance to represent the uniform ground states of Eq. (1).

VI. DISCUSSION

We find that the combined search using the fermionic mean-field theory and Gutzwiller projection yields chiral spin liquid states (both uniform and staggered flux types) with ordered chiralities as the likely ground states of the $S=1/2$ Heisenberg spin Hamiltonian on the pyrochlore lattice. Previous theories based on the perturbative expansion around the single-tetrahedron solution[1–5] did not find such chiral spin states. Given the past claims of dimer instability, a simultaneous search for a pronounced chirality and dimer correlations in the exact diagonalization of Eq. (1) will be valuable in sorting out the contending perspectives. The Fermi-level degeneracy one finds in the uniform flux state may have interesting consequences that will need to be explored more carefully in the future.

Note added. Recently, there appeared a preprint[12] pertaining to the chiral spin state on pyrochlore lattice. Its conclusions overlap with those here.

ACKNOWLEDGMENTS

H.J.H. thanks Dung-Hai Lee and Ashvin Vishwanath for discussions. This work was supported by the Korea Research Foundation Grant (Grants No. KRF-2008-521-C00085 and No. KRF-2008-314-C00101) and in part by the Asia Pacific Center for Theoretical Physics.

*hanjh@skku.edu

[1] B. Canals and C. Lacroix, Phys. Rev. Lett. **80**, 2933 (1998); Phys. Rev. B **61**, 1149 (2000).

[2] A. B. Harris, J. Berlinsky, and C. Bruder, J. Appl. Phys. **69**, 5200 (1991).

[3] H. Tsunetsugu, J. Phys. Soc. Jpn. **70**, 640 (2001); Phys. Rev. B **65**, 024415 (2001).

[4] E. Berg, E. Altman, and A. Auerbach, Phys. Rev. Lett. **90**, 147204 (2003).

[5] R. Moessner, S. L. Sondhi, and M. O. Goerbig, Phys. Rev. B **73**, 094430 (2006).

[6] R. Shankar, F. J. Burnell, and S. L. Sondhi, Ann. Phys. (N.Y.) (to be published).

[7] Ying Ran, Michael Hermele, Patrick A. Lee, and Xiao-Gang Wen, Phys. Rev. Lett. **98**, 117205 (2007); M. Hermele, Y. Ran, P. Lee, and X. Wen, Phys. Rev. B **77**, 224413 (2008).

[8] X. G. Wen, Frank Wilczek, and A. Zee, Phys. Rev. B **39**, 11413 (1989).

[9] Daniel S. Rokhsar, Phys. Rev. B **42**, 2526 (1990).

[10] Daniel S. Rokhsar, Phys. Rev. Lett. **65**, 1506 (1990).

[11] C. Gros, Ann. Phys. (N.Y.) **189**, 53 (1989).

[12] F. J. Burnell, Shoibal Chakravarty, and S. L. Sondhi, arXiv:0809.0528 (unpublished).